Research Article
The Journal of Comparative Neurology
Research in Systems Neuroscience
DOI 10.1002/cne.23714

Dendrodendritic Synapses in the Mouse Olfactory Bulb External Plexiform Layer

Dianna L. Bartel[1], Lorena Rela[2], Lawrence Hsieh[1], Charles A. Greer[1,3*]

Departments of [1]Neurosurgery and [3]Neurobiology, Yale University School of Medicine, 333 Cedar Street, New Haven, CT 06520-8082
Department of [2]Physiology and Biophysics, Systems Neuroscience Section, School of Medicine, University of Buenos Aires, and IFIBIO Houssay – CONICET, Calle Paraguay 2155, Buenos Aires, C1121ABG Argentina

Abbreviated running title: Dendrodendritic synapses of mouse EPL
Figures: 5
Tables: 1
Keywords: Dendrodendritic synapse, external plexiform layer (EPL), gephyrin, IMSR_JAX:014130; nif-0000-30467; nif-0000-00314; rid_000081; AB_887717; AB_300798; AB_1501344; AB_141596; AB_141357; AB_10562715; AB_2336881; AB_2314341

Grant Support: NIH DC00210 and DC01244 to C.A.G.

Author Contributions: DLB helped design the study, performed experiments, analyzed the data, and wrote the first draft of the manuscript. LR and LH carried out many of the whole cell recordings/dye fillings and contributed to the corresponding data analysis. CAG conceived the concept of this study, and contributed to the experimental design and analysis of data. All authors were involved in revisions of the draft manuscript and have agreed to the final content of the manuscript.

Conflict of Interest Statement: The authors have no known conflicts of interest in relation to this publication.

*Address correspondence to:

Charles A. Greer, Ph.D.
Department of Neurosurgery
Yale University School of Medicine
P.O. Box 208082
New Haven, CT 06520-8082
email – charles.greer@yale.edu

ACKNOWLEDGEMENTS

Received: Oct 07, 2014; Revised: Nov 18, 2014; Accepted: Nov 20, 2014

We thank Christine Kaliszewski and Dolores Montoya for expert technical assistance, and all members of the Greer lab for insightful discussions and critical reading of the manuscript.

ABSTRACT

Odor information relayed by olfactory bulb projection neurons, mitral and tufted cells (M/T), is modulated by pairs of reciprocal dendrodendritic synaptic circuits in the external plexiform layer (EPL). Interneurons, which are accounted for largely by granule cells, receive depolarizing input from M/T dendrites and in turn inhibit current spread in M/T dendrites via hyperpolarizing reciprocal dendrodendritic synapses. Because the location of dendrodendritic synapses may significantly affect the cascade of odor information, we assessed synaptic properties and density within sublaminae of the EPL and along the length of M/T secondary dendrites. In electron micrographs the M/T to granule cell synapse appeared to predominate and were equivalent in both the outer and inner EPL. However, the dendrodendritic synapses from granule cell spines onto M/T dendrites, were more prevalent in the outer EPL. In contrast, individual gephyrin-IR puncta, a postsynaptic scaffolding protein at inhibitory synapses used here as a proxy for the granule to M/T dendritic synapse was equally distributed throughout the EPL. Of significance to the organization of intrabulbar circuits, gephyrin-IR synapses are not uniformly distributed along M/T secondary dendrites. Synaptic density, expressed as a function of surface area, increases distal to the cell body. Furthermore, the distributions of gephyrin-IR puncta are heterogeneous and appear as clusters along the length of the M/T dendrites. Consistent with computational models, our data suggest that temporal coding in M/T cells is achieved by precisely located inhibitory input and that distance

from the soma is compensated with an increase in synaptic density.

INTRODUCTION

Olfaction begins when odorants bind to odorant receptors on olfactory sensory neurons in the olfactory epithelium (Buck and Axel, 1991). In mice, each sensory neuron expresses only 1 of the ~1,200 receptors (Zhang and Firestein, 2002) and projects an axon centrally to the olfactory bulb where it coalesces into a glomerulus (Mombaerts et al., 1996; Treloar et al., 2002). Axons from neurons expressing the same odorant receptor converge into 2-3 of the ~3,700 glomeruli (Richard et al., 2010) where they make excitatory synapses onto primary dendrites of the output neurons, mitral and tufted (M/T) cells. The M/T neurons, in turn, project their axons to a variety of cortical targets, apparently without the benefit of a well-defined odor-topography (Miyamichi et al., 2011; Sosulski et al., 2011; Igarashi et al., 2012). Prior to the cortical relay, the output of M/T neurons is sculpted by local olfactory bulb interneurons.

In addition to the single primary apical dendrite, M/T neurons extend several sparsely branched secondary dendrites laterally throughout the external plexiform layer (EPL) (Mori et al., 1983; Ke et al., 2013). Along these secondary dendrites reciprocal dendrodendritic synapses are formed, which are most widely described for the granule cell dendritic spines (Hinds and Hinds, 1976b; a; Sassoe-Pognetto et al., 2011). At the sites of dendrodendritic synapses, glutamate released from M/T dendrites depolarizes the granule cell spine, which in turn releases γ-aminobutyric acid (GABA) that can locally inhibit current spread in the M/T secondary dendrite (Xiong and Chen, 2002). The roles of interneuron GABAergic release onto M/T dendrites remains a question of interest but may include narrowing receptive fields and enhancing tuning specificity, synchronizing M/T firing, providing perceptual contrast enhancement, and modulating the gain of

olfactory bulb output (Yokoi et al., 1995; Luo and Katz, 2001; Schoppa and Urban, 2003; Tan et al., 2010; Kato et al., 2013; Miyamichi et al., 2013).

Dendrodendritic synapses were originally identified between mitral cell secondary dendrites and granule cell dendritic spines (Rall et al., 1966; Jackowski et al., 1978; Shepherd et al., 2004). However, there is increasing recognition of other interneuron populations throughout the EPL that also help shape odor activity via dendrodendritic synapses with M/T neurons (Toida et al., 1994; Lepousez et al., 2010; Huang et al., 2013; Kato et al., 2013; Miyamichi et al., 2013). The functional dynamics of dendrodendritic microcircuits are generally agreed upon (Shepherd et al., 2004). Computational models predict that mitral cell spike synchrony is modulated by the location of the dendrodendritic synapses on secondary dendrites (McTavish et al., 2012). However, the distribution of dendrodendritic synapses across the sublaminae of the EPL or along the length of M/T secondary dendrites has not been empirically explored. Therefore, in the current study we sought to understand the distribution of olfactory bulb local circuits within the EPL and to obtain accurate reconstructions of M/T secondary dendrites and the organization of synapses along the length of these dendrites. These data provide new insight into the cellular mechanisms shaping the receptive fields of the olfactory output projection neurons.

MATERIALS AND METHODS

Animals

Experiments were conducted on both male and female mice. CD-1 mice were obtained from Charles River Laboratories (Wilmington, MA). The Tg(Thy1-YFP)GJrs

mice were kindly provided by Dr. Feng at Duke University and subsequently bred in-house. These mice, which are available at JAX (RRID:IMSR_JAX:014130), were generated by random insertion and express the transgene containing YFP driven by the Thy1 promoter. The mice are on a C57B6/CBA background and expression is hemizygous (Feng et al., 2000). Animals were housed on a 14-hour light cycle with access to standard chow *ad-libitum*. The Yale University Animal Care and Use Committee approved animal use and procedures.

Perfusion and fixation

Animals were deeply anesthetized with an intraperitoneal injection of Euthasol (80mg/kg; Virbac, Fort Worth, Texas). The mouse was then perfused transcardially with 10 mL of 0.1M phosphate buffer saline (PBS; pH 7.4) plus heparin (1unit/mL) followed by 25 mL of 4% paraformaldehyde (in PBS, pH 7.4). The olfactory bulbs were removed from the skull and postfixed in the same fixative for two hours.

Immunohistochemistry

After washing in PBS for ten minutes, the tissue was blocked for 1 hour (3% bovine serum albumin, 0.3% triton, 5% normal donkey serum in PBS). The tissue was incubated overnight at 4°C with primary antibodies diluted in blocking solution: anti-gephyrin (1:750) and anti-GFP (1:1,000) or anti-Lucifer Yellow (1:1000). The following day, the sections were washed several times in PBS before incubating for two hours with the Alexa555 anti-mouse, Alexa488 anti-chicken or Alexa488 anti-rabbit, and DRAQ5

(1:1,000 each in blocking solution). The tissue was again washed in PBS before mounting and/or applying coverslips with Fluoro-Gel (EM Sciences; Hatfield, PA).

Antibody details and characterization

Further details for primary antibodies including species, clonality, manufacturer, catalog number, Research Resource IDentifier (RRID number; http://scicrunch.com/resources), and working dilution are listed in Table 1.

Gephyrin – Staining for gephyrin was used to identify the postsynaptic site of the inhibitory symmetric synapse from interneurons onto M/T dendrites. This monoclonal antibody recognizes the brain specific 93kDa splice variant on crude synaptic membrane fractions of rat brain (manufacturer's data sheet). The gephyrin staining in the current study is consistent with the staining pattern in the olfactory bulb previously described (Panzanelli et al., 2005).

Green fluorescent protein – The GFP antiserum was used to amplify the endogenous YFP signal in the Thy1-YFP-G tissue; as per the manufacturer data sheet this antibody recognizes all fluorescent proteins derived from the jellyfish *Aequorea victoria*. This antibody was verified by Western blot analysis and immunohistochemistry on brain tissue from transgenic GFP-expressing mice, in which the antibody staining co-labeled with the endogenous GFP (manufacturer's data sheet). This antibody was also tested in current experiments in non-YFP expressing mouse olfactory bulb tissue; no label was detected (data not shown).

Lucifer Yellow – The Lucifer Yellow antibody has been used previously and shown to specifically label cells filled with Lucifer Yellow (Zhang et al., 2006; Schmidt

and Kofuji, 2011). In addition, this antibody was tested in current experiments in tissue without Lucifer Yellow injection where no label was detected (data not shown).

Secondary antibodies and other stains – To test the specificity of secondary antibodies, they were applied to the tissue without the primary antibodies. No specific signal was detected confirming that the secondary signal normally results when it is bound to the primary antibody (data not shown). A fluorescently conjugated streptavidin was used to visualize the neurobiotin and nuclei were stained with DRAQ5.

Tissue processing

Electron microscopy

CD-1 mice, age 10 weeks, were perfused as described with 4% paraformaldehyde and 2% glutaraldehyde in PBS and the olfactory bulbs postfixed in the same fixative for 24 hours at 4°C. The tissue was processed for conventional electron microscopy as previously described (Montague and Greer, 1999; Au et al., 2002; Treloar et al., 2002). Briefly, olfactory bulb sections were treated with osmium tetroxide, dehydrated through graded alcohols and polymerized in EPON between glass slides and coverslips that were coated with Liquid Release Agent (EM Sciences). Smaller regions containing the EPL were micro-dissected from EPON blocks and sectioned at 0.07µm.

Tg(Thy1-YFP)GJrs

After perfusing and postfixing the olfactory bulbs from the YFP animals, age 10 weeks, the tissue was cryoprotected with 30% sucrose in PBS overnight at 4°C. The next day the tissue was mounted in Optimal Cutting Temperature compound (Fisher,

Pittsburgh, PA). The bulbs were cut on a cryostat at 20μm slices that were collected directly onto Superfrost slides (Fisher), which were stored at -20°C until they were stained with the anti-GFP and anti-gephyrin antibodies and DRAQ5.

Lucifer Yellow injections

These injections were carried out as previously described (Imamura and Greer, 2009). Briefly, CD-1 animals at 4 weeks of age were perfused as described. Following two-hour post fixation, the olfactory bulbs were embedded in 1.5% agarose and 300μm free-floating sections were collected on a vibratome. The slices were mounted onto a membrane filter and placed into a chamber with a solution of phosphate buffer (0.1M, pH 7.4). A solution of Lucifer Yellow (6% in 50mM Tris-HCl, pH 7.4: #L453, Invitrogen; Carlsbad, CA) was backfilled into a glass micropipette, which was placed in the mitral cell layer and the dye was injected with negative current (1- 10 nA) for 15 minutes. These slices were then postfixed in 4% paraformaldehyde overnight at 4°C before they were stained with the anti-Lucifer Yellow and anti-gephyrin antibodies and DRAQ5.

Dye filling of individual mitral cells

CD-1 animals between the age of 12 – 15 days postnatal were anesthetized with an injection of Euthasol and then perfused intracardially with 25 mL of ice-cold artificial cerebrospinalfluid (ACSF, in mM:118 NaCl, 3 KCl, 1.25 NaH_2PO_4, 26 $NaHCO_3$, 10 glucose, 2 $CaCl_2$, 1 $MgSO_4$, 0.4 ascorbic acid, 4 sodium lactic acid, and 2 sodium pyruvic acid; 300 mOsm, pH7.4; made fresh daily). In ice-cold ACSF equilibrated with 95% O_2/5% CO_2, the brain was rapidly dissected and 300μm coronal sections of the OB were

collected on a vibratome. The sections recovered in a chamber with oxygenated ACSF at room temperature for twenty minutes prior to recording. Then, the bulb slices were placed in a flow-through chamber mounted on an upright microscope (Olympus BX51WI), with continuous perfusion with oxygenated ACSF at room temperature. The tissue slices were visualized with differential interference contrast (DIC) illumination and 40× water-immersion objective (N.A. 0.9).

Whole-cell electrophysiological recordings were obtained with standard methods (Rela et al., 2010). Mitral cells were identified based on location in the mitral cell layer, size of soma, the presence of spontaneous action potentials and a membrane potential around -50mV. Pipettes were pulled from thin-walled borosilicate glass electrodes (Sutter Instruments, Novato, CA; #BF150-110-10) on a P-97 puller (Sutter) and had a resistance between 4–7 MΩ and when filled with internal solution [in mM: 4 KCl, 125 K-Gluconate, 10 HEPES, 10 Phosphocreatine, 1 EGTA, 0.2 $CaCl_2$, 4 Na_2-ATP, 0.3 Na-GTP and 0.5% neurobiotin (Vector Labs, Burlingame, CA; #SP-1120); 290 mOsm, pH7.4].

Recordings were done with a Multiclamp 700B amplifier (Molecular Devices, Sunnyvale, CA). Current signals were low-pass filtered (4 kHz) and digitized via Digidata 1440A (Molecular Devices). Under voltage clamp (holding potential at -50 mV), the cells were recorded for 10 minutes to allow for the neurobiotin to diffuse into the cell and the pipette was then carefully retracted.

The gephyrin staining in these acute slices was especially sensitive to the length of fixation, similar to a previous report (Schneider Gasser et al., 2006). The optimal time of fixation to allow for both neurobiotin and gephyrin staining was 20 minutes and all solutions for the following staining were made fresh daily.

After filling a mitral cell with neurobiotin, the tissue slice was immersed in 4% paraformaldehyde (in 0.1M phosphate buffered saline, pH 7.4) for 20 minutes at room temperature. After three twenty-minute washes in 0.1M phosphate buffered saline (PBS, pH 7.4), the section was incubated for one hour in blocking solution (0.3% triton and 5% normal goat serum in PBS). The slice was then incubated with the gephyrin antibody (1:750 in blocking solution) overnight at 4°C. The next day, three twenty-minute PBS washes were followed by 1-hour incubation with the Alexa555 anti-mouse secondary, Alexa488 streptavidin and DRAQ5 (1:1,000 each in blocking solutions) at room temperature. After several washes in PBS the tissue slice was mounted onto a glass slide and a coverslip was applied with Fluoro-Gel.

Electron micrograph acquisition and analysis

For ultrastructural analysis thin sections were examined with a JEOL 1200 electron microscope and photographed at primary magnifications of 10,000×. The negatives of electron micrographs were digitized on a flatbed scanner at 1200 dpi. Serial individual electron photomicrographs were taken throughout the entire width of the EPL from the inner glomerular layer to the mitral cell layer.

Using tissue from three different animals, five montages of serial EM images spanning the width of the EPL were constructed and analyzed. Synapses on M/T dendrites were identified based on stringent criteria and were then counted. Dendritic synapses were identified on the basis of clearly distinct membrane specializations, a definitive synaptic cleft separating the two processes, and the distribution and morphology of vesicles. The excitatory asymmetric synapses are polarized from M/T

dendrites onto interneuron spines with a thicker specialization postsynaptically on the interneuron spine. Further, the asymmetric synapses contain spherical vesicles closely apposed to the M/T dendritic membrane. The inhibitory symmetric synapses are polarized from the interneurons onto M/T dendrites with symmetrical pre- and postsynaptic specializations. The symmetric synapses contain oval shaped vesicles throughout the head of the interneuron spine. These total counts entail all identifiable dendrodendritic synapses regardless of whether the accompanying reciprocal synapse was found in the same image.

Among these total synaptic counts, we found 64 pairs of reciprocal synapses where the symmetric and asymmetric synapses were present in the same image. These reciprocal pairs were analyzed using ImageJ 1.64 (National Institutes of Health, Bethesda, MD; RRID:nif-0000-30467), where the length of the synaptic membrane specializations was measured and the number of vesicles counted. We restricted the vesicle number analysis to what we defined as the readily releasable pool, which considered a depth of 100nm from the membrane specialization. Therefore, our counts consisted of vesicles contacting the membrane specialization and the next adjacent layer of vesicles. The measurements were analyzed with one-way ANOVAs and post hoc analysis or t-tests.

Confocal image acquisition and analysis

All other tissue sections were imaged with a Leica TCS SL laser scanning confocal microscope (Leica Microsystems; Wetzlar, Germany). The red, green and blue channels were obtained sequentially and then merged together to prevent sideband

excitation of the fluorophores. Images were sampled at a resolution of 1024 by 1024 pixels with the pinhole set at 1 Airy unit and using 20× objective (N.A. 0.70) or 63× oil-immersion objective (N.A. 1.4). Puncta and dendrite analysis was performed on the original 8-bit images obtained with the 63× oil immersion objective and a digital zoom factor 3.0, yielding a resolution of ~0.2μm. Images in figure panels were adjusted for brightness in Adobe Photoshop CS5.

Tg(Thy1-YFP)GJrs analysis – Quantification of the size and number of gephyrin stained puncta was performed on single-plane confocal images obtained at 63× with a resolution of ~0.2μm. Using ImageJ 1.64, images were adjusted using a threshold for signal intensity that maximized the puncta signal and minimized inclusion of background signal, typically ~80 on a 0–255 gray-value scale. Within a 500μm^2 area of the EPL, we determined the number of gephyrin stained puncta with a size between 0.2μm^2 and 2μm^2, a range within our resolution limit.

For statistical analysis, both size as well as frequency of gephyrin puncta in the outer and inner EPL were examined in each of four anatomical regions (dorsal, ventral, medial, lateral). For each anatomical division, 3 images/animal were obtained and a total of 3 animals were analyzed. There were no significant differences in the size or frequency of puncta within these anatomical regions using a Kruskal-Wallis test for multiple comparisons. Therefore, within each animal the outer and inner EPL measurements were combined across the anatomical regions (i.e., 12 measures for each outer and inner). Although this non-stereological method could result in oversampling of

larger puncta (>0.5μm), they represent a small fraction of the total population as shown previously (Panzanelli et al., 2005 and see Figure 2D)

The distribution of gephyrin-IR puncta along YFP+ dendrites was also examined in the single-plane images in a total of 360 segments (120 segments for each of three animals). The length and diameter of YFP+ dendritic segments were measured manually in ImageJ. The length of YFP+ segments that could be identified and measured were 12μm or less and the diameter was consistent along the length of the segment (i.e., no tapering). Therefore, using the formula for the surface area of a circular cylinder, the surface area of dendritic segments was calculated by the following:

$$2*\pi*\text{radius dendrite}*\text{length dendrite}$$

The gephyrin puncta on these segments were manually determined based on location, puncta either entirely enclosed in or half of the puncta touching the YFP+ dendrite. Data from these dendrite segments were analyzed as a measure of the diameter of the dendrite. In this way, larger diameters represent segments closer to the somata while the thinner diameters are located more distally from the somata. The total number of gephyrin puncta and overall length or surface area of all dendritic segments were used to estimate the density of synapses according to dendritic length (linear) or surface area.

Lucifer Yellow injection analysis – We analyzed 37 dendritic segments from four different tissue slices, each from a different animal, labeled with Lucifer Yellow and stained for gephyrin. These slices were optically sectioned with confocal microscopy using the 63× immersion objective and a z-step size of 0.12μm. The length and diameter of dendrites were determined with ImageJ using the stacked projections with z-stack depths averaging ~8μm. The gephyrin puncta on these segments were again manually

determined based on location: puncta entirely enclosed or half of the puncta touching the Lucifer Yellow-filled dendrite. Data from these dendritic segments were also examined as a measure of dendrite diameter as we did with the YFP dendrites. Similarly, the number of gephyrin puncta was used to estimate the density of synapses according to dendritic length (linear) or surface area.

Individually labeled mitral cells analysis – We analyzed six individually labeled mitral cells, each from different animals, which were also stained for gephyrin. These slices were optically sectioned with confocal microscopy using the 63× immersion objective and 3.0 times software zoom. Using the z-stack file, we created a 3D surface rendering of the labeled dendritic segments with Imaris 6.2.1 (Bitplane, Saint Paul, MN; RRID:nif-0000-00314). The gephyrin staining was then filtered based on the reconstructed surface. This allowed for the removal of all gephyrin fluorescence that was extraneous to our labeled dendrites (as detailed in (Fogarty et al., 2013). This automatic detection of synapses in 3D space is based on both intensity and size. Therefore, we acquired the confocal z-stacks with a 0.12μm z-step interval, which was smaller than the average 0.5μm gephyrin puncta. This ensured that puncta were present in a minimum of two confocal optical slices and were not an artifact of the background subtraction.

In order to calculate the surface area of the dendrite as we did for the YFP and Lucifer Yellow analysis, we measured shorter segments of dendrite ≤100 μm in length that had a consistent diameter. The diameter was determined by taking the average of three measurements along the length of dendrite, the diameter was considered consistent when all three measurements were within 0.5μm of each other. The number of gephyrin

puncta that was determined with Imaris was used to calculate the density of synapses of either linear (length) or surface area density along the dendrite.

Statistical analysis

All data was analyzed and graphed using Graphpad6 software (La Jolla, CA; RRID:rid_000081). When possible, we used parametric comparisons based on *t* tests (for paired comparisons, i.e., inner EPL versus outer EPL) or ANOVA (for multiple comparisons, i.e., vesicle number, synapse length). If normality was not fulfilled due to small sample sizes, we used Mann–Whitney Wilcoxon rank sum tests. Significance was defined as $p<0.05$.

RESULTS

Within the EPL of the olfactory bulb, M/T secondary dendrites make reciprocal dendrodendritic synapses with interneurons, primarily the granule cells. The secondary dendrites of mitral cells are largely restricted to the inner portion of the EPL while those of tufted cells occupy most of the outer EPL (Mori et al., 1983; Orona et al., 1984). Similarly, subpopulations of granule cells have been described that appear to preferentially arborize in either the superficial or deep EPL (Mori et al., 1983; Orona et al., 1984; Greer, 1987). For these reasons, we divided the EPL spanning from glomerular layer to mitral cell layer into equal outer and inner laminae for analysis.

We began our investigation of sublaminar dendrodendritic synapse distribution with immunostaining for gephyrin. This postsynaptic scaffolding protein selectively localizes to GABAergic synapses (Sassoe-Pognetto and Fritschy, 2000) and served as a

proxy for identifying inhibitory synapses within the EPL. At dendrodendritic synapses the gephyrin is clustered in M/T dendrites, facing the release site formed by the granule cell dendritic spine (Panzanelli et al., 2009). Therefore, gephyrin-IR (immunoreactivity) could be effectively used as a representation of the postsynaptic membrane specialization on the M/T cell secondary dendrites.

At low magnification, gephyrin-IR was intense and uniform throughout the EPL with only moderate staining in the glomerular layer, mitral cell layer and granule cell layer (shown in magenta, Figure 1A). Inverted single-plane confocal images at higher resolution were used to quantify the distribution of gephyrin-IR in the outer and inner EPL (Figure 1B). This analysis revealed that the density of gephyrin-IR puncta was slightly but not significantly higher in the outer EPL (225 versus 212 punta/500μm^2, respectively; Figure 1C). These results are in alignment with a previous study examining gephyrin puncta size and distribution in the EPL in rats (Panzanelli et al., 2005) .The size of the gephyrin-IR puncta determined by cumulative and relative frequency revealed that the majority of puncta are 0.5μm^2, consistent throughout the EPL (Figure 1D; cf. Panzanelli et al., 2005).

We continued our investigation of sublaminar synapse distribution by montaging serial electron micrographs that spanned the entire width of the EPL. At the ultrastructural level the dendrodendritic synapses have a characteristic appearance. The M/T to interneuron synapse, the asymmetric synapse, is defined by small pools of spherical vesicles closely apposed to the presynaptic membrane of the M/T dendrite and an asymmetrically thick membrane specialization on the interneuron cell spine. The reciprocal synapse from the interneuron onto the M/T, the symmetric synapse, is defined

by large pools of elliptically shaped vesicles within the spine head and symmetrical thickenings on both the presynaptic and postsynaptic membranes (Figure 2A, boxed inset).

In tissue processed for conventional transmission electron microscopy, the dendritic profiles were easily identified. The M/T dendrites were large electron lucent profiles with relatively smooth profiles and regular arrays of microtubules (pseudo colored purple in Figure 2B, C). In contrast, the dendritic spines of interneurons were smaller electron dense profiles often with irregular outlines (Figure 2B, C; pseudo colored yellow). The excitatory asymmetric synapse contained small spherical vesicles in the M/T dendrite that were closely apposed to the presynaptic membrane, which was accompanied by an asymmetrically thickened membrane specialization on the spine head. The inhibitory symmetric synapse appeared with large clusters of elliptically shaped vesicles and symmetrical thickenings of both the pre- and postsynaptic membranes. In optimal sections, reciprocal pairs of asymmetric and symmetric synapses were seen adjacent to one anther (see examples in Figure 2Bi, ii).

We first counted the number of asymmetric and symmetric synapses throughout the outer and inner EPL regardless of their reciprocity. The density of asymmetric synapses was significantly greater than that of symmetric synapses in the outer and inner EPL (Figure 1D, E). Specifically, in the outer EPL asymmetric synapses averaged 10.1 ± 0.47 synapses/100μm^2 compared to symmetric synapses with 5.25 ± 0.32 synapses/100μm^2 ($p<0.0001$); in the inner EPL asymmetric synapses averaged 9.3 ± 0.45 synapses/100μm^2 versus the symmetric synapses with 3.44 ± 0.25 synapses/100μm^2 ($p<0.0001$). The density of asymmetric synapses throughout the outer and inner EPL was

consistent (i.e., 10.1 and 9.3 synapses/100μm^2, respectively). The symmetric synapses, however, varied with a significantly higher density in the outer EPL compared inner EPL (5.25 versus 3.44 synapses/100μm^2, respectively; $p<0.0001$).

From among the large population of synapses, we identified 64 reciprocal synaptic pairs. In these we quantified the length of the specialized membranes and the number of vesicles adjacent to the membrane specialization, which we defined as the readily releasable zone. The average length of the membrane specialization at symmetric synapses was greater than that of the asymmetric membrane specialization (Figure 2F). In the outer EPL, symmetric specializations averaged 397 ± 23.4 nm while the asymmetric specializations averaged 309 ± 16.3 nm ($p<0.0001$). Similarly, in the inner EPL the symmetric specializations were 389 ± 33.6 nm and the asymmetric specializations were 264 ± 18.5 nm ($p<0.01$). This difference in length was observed in 70% of the reciprocal pairs examined in the inner EPL. That is to say, 14 of the 20 pairs examined in the inner EPL had longer symmetrical than asymmetrical membrane specializations. Similarly, 75% (33 of the 44 examined) of reciprocal pairs in the outer EPL had longer symmetrical synapses. It is noteworthy that the electron microscopy linear measurements of the symmetrical synaptic membrane specialization are consistent with the diameters of the gephyrin –IR puncta identified with the high resolution confocal microscopy. The gephyrin-IR puncta we have measured suggest the localization of multiple gephyrin molecules at individual inhibitory synaptic sites, as previously suggested by Specht et al. (2013). The symmetric synapses also had more vesicles than the asymmetric synapses on average (Figure 2G) as well as in pairs (75% in inner EPL and 77% in outer EPL). These data suggest that there is a reciprocity of synaptological features of the symmetrical and

assymmetrical dendrodendritic synapses, which can be equated with synaptic strength (Schikorski and Stevens, 1999).

Sampling limitations make electron microscopy an impractical analysis for longitudinal distribution of dendrodendritic synapses on the secondary dendrites. Therefore, we used gephyrin-IR puncta to assess the distribution of the inhibitory synapses along the length of the secondary dendrites. Though gephyrin-IR slightly overestimates the number of symmetric synapses compared to the ultrastructural analysis, it served as a general proxy for locations of dendrodendritic reciprocal synaptic pairs that we could analyze in relation to labeled M/T dendrites.

We initiated this analysis with the Tg(Thy1-YFP)GJrs mice, where subsets of M/T cells express YFP under the Thy1 promoter (Feng et al., 2000; Imamura and Greer, 2009). In these mice, YFP is expressed in the M/T cell bodies as well as throughout the apical and secondary dendrites (Figure 3A). Mitral cell somata are found in a discreet layer (the mitral cell layer, MCL) located a few hundred microns from the glomerular layer and have their secondary dendrites distributed predominately in the inner EPL. In contrast, tufted cell somata are located in the EPL with secondary dendrites localizing primarily to the outer EPL (Mori et al., 1983). Mitral and tufted cells also differ in their axonal and dendritic projection patterns (Nagayama et al., 2010; Igarashi et al., 2012). However, they both form dendrodendritic synapses with interneurons. The density of YFP+ dendrites in the outer EPL is lower than in the inner EPL, which might reflect a preferential labeling of mitral cells over the tufted cells. Regardless, the YFP labeled dendrites in both the outer and inner EPL were suitable for our purposes of analyzing individual dendritic segments. In single-plane confocal images at high resolution,

individual YFP+ dendritic segments could be identified (Figure 3B). The gephyrin-IR puncta associated with the segments of interest were determined in addition to measuring the length and diameter of dendritic segments (Figure 3C, C'). Using these measurements, we analyzed the density of synapses along dendritic segments as a function of dendrite diameter. In this way, segments with the larger diameter, upwards of 2.5μm, represent proximity to the soma while segments with smaller diameters are progressively distal to the soma. When the number of gephyrin-IR puncta was divided by the available length of a dendritic segment the calculated linear density was greater proximally than distally, i.e., segments with a larger diameter had a greater number of synapses per unit length (Figure 3D). This pattern of linear density was similar in both the outer and inner EPL. However, dendrites are not symmetrical cylinders with a constant diameter. Rather, the diameter of dendrites tapers toward the terminal ends (Cuntz et al., 2007; Donohue and Ascoli, 2008). As such, the proximal dendritic segments expose a larger surface area available for synaptic inputs, i.e., "synaptic space". Thus, we considered gephyrin density in relation to the entire area available for synaptic contact. When the number of gephyrin-IR puncta was divided by the surface area of a dendritic segment, we found a higher density of synapses on the segments with smaller diameters and hence, further from the cell body (Figure 3E).

While the Tg(Thy1-YFP)GJrs model provided extensive labeling of M/T dendrites throughout the EPL, this was a hindrance to following an individual dendrite for more than ~ 12μm. Therefore, we sought to examine smaller populations of labeled M/T dendrites by iontophoretically injecting Lucifer Yellow dye into the mitral cell layer of fixed olfactory bulb slices. These injections resulted in the labeling of subsets of cells

in the vicinity of the pipette (Figure 4A). At higher magnification of this tissue, we could identify and measure individual Lucifer Yellow-labeled M/T dendritic segments and the associated gephyrin-IR puncta (Figure 4B). Even though these injections also labeled a subset of granule cells due to their high density in the mitral cell layer (Imamura et al., 2006), the spiny appearance of granule cell dendrites made them easy to distinguish from the M/T dendrites of interest (Figure 4B arrow). The Lucifer Yellow-labeled secondary dendrites of interest were largely restricted to the inner EPL given placement of the pipette. This labeling technique allowed us to follow individual dendritic segments for longer distances throughout the depth of the tissue. In z-stack projections we identified the gephyrin-IR puncta along the Lucifer Yellow+ dendrites of interest (Figure 4C, C'). As with the YFP+ dendrites in the previous experiment, the gephyrin density was analyzed first as a function of dendrite diameter. The linear density revealed that distribution of gephyrin-IR synapses averaged 1.94 synapses/μm along dendrites regardless of dendrite diameter, i.e., the slope of the best-fit line was not significantly different than 0. (Figure 4D). Yet when we considered the "synaptic space" of the segment and determined the gephyrin-IR density in terms of the dendritic surface area we again found that the synaptic density was higher on segments with a smaller diameter (i.e., more distal to the somata; Figure 4E).

Using two different methods to label M/T dendrites, our data thus far indicate that the density of gephyrin-IR puncta as a function of dendritic diameter is greater at sites more distal to the soma of M/T cells. To pursue this further we turned to electrophysiological methods in order to fill individual mitral cells with neurobiotin. Using acute slices, mitral cells were readily identified based on their large somata size

(10-20μm), location in the mitral cell layer, a resting membrane potential near -50mV and spontaneous action potentials (Figure 5A). Mitral cells were filled with neurobiotin under voltage clamp for 10 minutes, after which the slices were stained with streptavidin-A488, anti-gephyrin, and DRAQ5 (shown in green, red, and blue, respectively; Figure 5B).

Our aim was to reconstruct mitral cell secondary dendrites and map their inhibitory synaptic input. To achieve this, we used confocal microscopy to optically section the entire filled mitral cell, which was largely confined to the upper 40μm of the section (Figure 5B). These z-stack images were used with Imaris software to create a detailed surface rendering of the neurobiotin-filled mitral cell (Figure 5C). The gephyrin-IR in the red channel was then filtered based on the neuronal surface so that only the signal that was continuous with the mitral cell surface was conserved (see methodological details in Fogarty et al., 2013). From the filtered gephyrin-IR channel, the number of puncta along dendritic segments was automatically determined and modeled with the dendritic surface. Hence, the single cell fills enabled us to examine the distribution of gephyrin-IR puncta at high resolution and for much longer distances along the secondary dendrites. This revealed an additional feature of synaptic organization. Namely, the distribution of puncta was not uniform or homogeneous along the dendritic length (Figure 5D1-4, E1-4; gephyrin puncta shown in magenta). Puncta appeared heterogeneously and in small clusters with intervening domains that did not show evidence of synaptic specializations. This observation is reminiscent of reports detailing synaptic clusters (Druckmann et al., 2014; Rotterman et al., 2014) and consistent with the notion that

receptive fields of the secondary dendrites may have spatially defined attributes that contribute to odor information processing (Migliore et al., 2010; McTavish et al., 2012).

In order to calculate the length and surface area of these dendrites as we did for the previous analyses, we measured shorter segments (≤100 μm in length) that had a consistent diameter. We analyzed a total of six filled mitral cells in this manner and with these measurements obtained linear and surface density of gephyrin as a measure of dendrite diameter (Figure 5F, G). These data were consistent with our prior measurements in the YFP mice and following Lucifer Yellow injections. These results provide further evidence that the linear density of gephyrin-IR is consistent along dendrites, in this case averaging 1.1 synapses/μm. Conversely, the surface area density reveals a higher synaptic density on the terminal segments. Thus, using various methods to label M/T dendrites, our data consistently show that gephyrin density expressed as a function of surface area increases distal to the cell body.

DISCUSSION

Reciprocal dendrodendritic synapses between the secondary dendrites of M/T cells and the dendritic spines of interneurons, primarily granule cells, modulate odor information. Here, we examined their distribution in sublaminae of the EPL and along the length of isolated secondary M/T dendrites. Using a high resolution mapping of gephyrin-IR, as a proxy for reciprocal synapses, we determined the density of dendrodendritic synapses along the secondary dendrite proximal and distal to the soma. Our analyses demonstrate that the distribution of dendrodendritic synapses is comparable in the outer and inner sublaminae of the EPL, their distribution along individual M/T

dendrites is heterogeneous. First, while the absolute density of appositions (i.e., linear density) is relatively constant along the length of dendrites, they appear in clusters with intervening membrane devoid of synaptic specializations. Second, the surface area density of synapses increases distally as the dendrite tapers toward the terminal end.

Analysis of EPL synapses

To identify dendrodendritic synapses within the EPL, we utilized staining for gephyrin. This postsynaptic scaffolding protein selectively localizes to GABAergic synapses (Sassoe-Pognetto and Fritschy, 2000) and has been used extensively in the analysis of dendrodendritic synapses in the EPL specifically (Panzanelli et al., 2005; Panzanelli et al., 2009; Pallotto et al., 2012). Similar to these previous studies, we found that gephyrin-IR was distinctly punctate and uniform throughout the extent of the EPL.

We furthered these analyses of dendrodendritic synaptic distribution throughout the EPL at the ultrastructural level. In our electron micrograph montages, we used strict criteria to identify dendritic symmetric and asymmetric membrane specializations. Our total synaptic counts, regardless of their reciprocity, showed greater numbers of asymmetric than symmetric synapses. Yet the dendrodendritic synapses throughout the EPL are agreed to be almost entirely reciprocal (Woolf et al., 1991). The challenge of consistently imaging the reciprocal pair in a single electron micrograph is likely due in part to the plane of section and the difficulty of unequivocally identifying the symmetric specializations compared to the more obvious asymmetrical thickenings. Taken together with the uniform gephyrin-IR, it is possible that the gephyrin staining detects intracellular gephyrin that is not yet fully integrated into synaptic membranes and/or unoccupied

synaptic specializations that might be expected based on the ongoing turnover of the olfactory bulb granule cells (Whitman and Greer, 2009).

Olfactory bulb granule cells are continuously generated in the subventricular zone after which they integrate into olfactory bulb circuits. Deep granule cells, whose dendrites preferentially arborize in the inner EPL, turn over more frequently in adults than do superficial granule cells (Lemasson et al., 2005). Developmentally, Hinds and Hinds (1976b) speculated in the neonate that the excitatory asymmetric synapse formed prior to the reciprocal symmetric synapse. Similarly, Kelsch et al. (2008) suggested that in adult born granule cells the excitatory glutamatergic synapse onto granule cell apical dendrites formed prior to the reciprocal inhibitory synapse. Our lower estimate of reciprocal synapses in the inner EPL may reflect a granule cell population that is more transient or immature than those targeting the outer EPL. Likewise, we previously showed that adult-born granule cells are first innervated by axon collaterals prior to integrating into EPL dendritic circuitry (Whitman and Greer, 2007). The current data we report here are consistent with the notion that there is pause between the formation of excitatory and inhibitory synapses along the secondary dendrites.

The analysis of reciprocal dendrodendritic pairs illuminates the variability of synaptic details within the paired unit. In particular, the number of vesicles and the length of the symmetric membrane specialization were both greater than those of the asymmetric synapses throughout the EPL. These measures can infer synaptic strength. For instance, cortical synapses show tight correlations between synaptic strength and the surface area of the postsynaptic density and the total number of presynaptic vesicles (Harris and Weinberg, 2012) as well as the number of docked vesicles (Lisman and

Harris, 1993; Schikorski and Stevens, 1997; 1999). Furthermore, the probability of vesicle release increases as a function of the number of docked vesicles (Dobrunz and Stevens, 1997; Murthy et al., 1997). While these analyses have been based on axodendritic synapses, it is tempting to speculate that our data suggest that symmetric synapses within reciprocal pairs exert a comparatively stronger influence and that this inhibition may be greater in the outer EPL than in the inner EPL.

Inhibitory synaptic distribution along M/T dendrites

Recent studies shed light on the diversity of GABAergic interneurons in the EPL, some of which form dendrodendritic synapses with M/T neurons (Pressler and Strowbridge, 2006; Parrish-Aungst et al., 2007; Eyre et al., 2008). Notably, parvalbumin expressing interneurons appear to make reciprocal dendrodendritic synapses with M/T dendrites (Toida et al., 1994; Kosaka and Kosaka, 2008). Given that our analysis did not discriminate between granule cells and other interneuron types, synapses made by these interneurons were undoubtedly included in our analyses. However, granule cells, at a density of $10^5/mm^3$ (Richard et al., 2010) outnumber other populations of olfactory bulb interneurons, conservatively, by 100:1 (Lledo et al., 2008). Thus it seems reasonable to propose that the data we report here are largely representative of granule cell to M/T neuron interactions.

Using three different methods to label M/T cell secondary dendrites combined with gephyrin staining generated results consistent across all three approaches. The density of gephyrin-IR puncta as measured by surface area increased as the dendrites tapered distally from the cell soma. The gephyrin-IR puncta often appeared

heterogeneously distributed in clusters across the surface of the secondary dendrites. Proximal to the soma, or among the largest diameter dendritic segments, we found less evidence of clustering. Rather, gephyrin-IR puncta proximal to the soma appeared to be more isolated from their nearest neighbor puncta. This might suggest that interneurons targeting dendrites proximal to the soma establish isolated synapses whereas those targeting branches distal to the soma establish small synaptic networks mediated by clustered synapses. The mechanisms underlying the heterogeneous distribution and clustering of synapses is not known but may reflect developmental mechanisms. For example, hippocampal synaptic networks show evidence of differential stability or strengthening of synapses at different points in the dendritic arbor as a function of activity (Steward et al., 1998). The heterogeneous synaptic distribution on M/T dendrites may reflect granule cell turnover, and therefore synaptic turnover, in relation to their connection with M/T cells. It is intriguing that the proximal to distal densities of gephyrin-IR puncta were equivalent in the outer and inner EPL. There is a general consensus that mitral cell secondary arbors are largely restricted to the inner EPL while tufted cell arbors remain in the outer EPL (Mori et al., 1983). The Lucifer Yellow and neurobiotin labeling specifically targeted mitral cells, while the Tg(Thy1-YFP)GJrs labeled both mitral and tufted cells, albeit the latter less heavily (cf. Figure 3 and the paucity of YFP labeling in the outer EPL). This suggests that mechanisms regulating the distribution of dendrodendritic complexes are similar for mitral and tufted cells.

As noted above, recent reports underscore the diverse types of interneurons in the olfactory bulb, which also contribute to local circuitry (Pressler and Strowbridge, 2006; Parrish-Aungst et al., 2007; Eyre et al., 2008). Of these interneurons, those expressing

parvalbumin are broadly connected to M/T cells, consistent with their broad odor tuning, compared to the more narrowly-tuned and perhaps more narrowly connected granule cells (Kato et al., 2013; Miyamichi et al., 2013). These observations imply that the synapses on the most distal dendrites in our analysis reflect those of the parvalbumin interneurons while the synapses more proximal to the M/T soma may be derived from granule cells.

Functional considerations

The temporal and spatial shaping of olfactory bulb output is strongly influenced by dendrodendritic inhibition. The reciprocity and synaptic arrangement of dendrodendritic synapses underlies odor discrimination by way of sharpening odor tuning and enhancing contrast (Lagier et al., 2007). Following primary afferent excitation, action potentials in M/T neurons actively propagate along the dendrites. The primary apical dendrites within the glomerulus have a high concentration of sodium channels and action potentials propagate along their length without attenuation (Bischofberger and Jonas, 1997; Chen et al., 1997). Similarly, action potentials actively propagate to the distal ends of the secondary M/T dendrites (Bischofberger and Jonas, 1997; Xiong and Chen, 2002) though there may be exceptions (Margrie et al., 2001). Glutamate release from these secondary dendrites requires substantial depolarization (Xiong and Chen, 2002) and activation of high-threshold calcium channels (Isaacson and Strowbridge, 1998), triggering the reciprocal GABA release from the interneuron dendritic spines. The inhibitory synaptic input that is recruited following an action potential regulates the extent of action potential propagation along the lateral dendrites (Xiong and Chen, 2002).

The distal segments of secondary dendrites are likely less influenced by back-propagated action potentials and more likely to participate in local dendrodendritic microcircuits. Likewise, the inhibition from the distal synapses would have a weaker influence on action potentials initiation at the soma. Hence, the distal inhibitory synapses might correspond to compartments of the secondary dendrites predominantly participating in microcircuits. Similar microcircuits have been described in cortical pyramidal neurons where inhibitory synapses are locally clustered along dendritic spines and shafts (Chen et al., 2012) and within ~10μm of each other, the spatial range of local intracellular signaling mechanisms (Golding et al., 2002; Major et al., 2008). The role of the distant synaptic microcircuits on M/T secondary dendrites seems most compatible with lateral inhibition. Conversely, the proximal inhibitory input would drive temporal coding, such as synchronized M/T firing (Kashiwadani et al., 1999; Nusser et al., 2001; Lagier et al., 2004; Lagier et al., 2007). The synaptic distribution that we present here suggests that temporal coding is achieved by precisely located inhibitory input, as is predicted from network models (McTavish et al., 2012), while the lateral inhibition requires more synaptic strength, in terms of greater synaptic density.

FIGURE LEGENDS

Figure 1. Inhibitory synaptic distribution throughout the external plexiform layer (EPL) as seen by staining for gephyrin, a post-synaptic marker of GABAergic synapses. **A.** Gephyrin-IR (immunoreactivity, in magenta) appears punctate and uniform throughout the EPL. Layers within the olfactory bulb are visualized and delineated with the DRAQ5 nuclear stain (green). **B.** Staining from boxed region in panel A; Gephyrin was imaged at higher resolution and the gray-scale inverted images were used to analyze puncta. **C.** The density of gephyrin-IR puncta is uniform across the outer EPL (black bar) and inner EPL (grey bar). **D.** The mean size of gephyrin-IR puncta is 0.5μm; cumulative and relative frequencies are also shown.
Error bars indicate SEM. Abbreviations: GL, glomerular layer; EPL, external plexiform layer; MCL, mitral cell layer; GCL, granule cell layer.

Figure 2. Dendrodendritic synapses in the EPL. **A.** A simplified circuit of the olfactory bulb. The mitral/tufted cells (M/T; purple) extend their primary dendrite into glomeruli where they receive input from the axon terminals of olfactory sensory neurons. Along the M/T secondary dendrites, which extend laterally through the EPL, dendrodendritic synapses are formed with interneurons (yellow). These synapses occur primarily with granule cells, located deep in the granule cell layer, and possibly with various interneuron populations within the EPL. *Box inset:* The dendrodendritic microcircuit begins at the asymmetric synapses with the M/T release of glutamate onto interneuron dendritic spines. This synapse is defined by vesicles closely apposed to the M/T presynaptic membrane and an asymmetrically thick post-synaptic specialization on the interneuron membrane. The reciprocal symmetric synapse entails vesicle clusters throughout the spine of the interneuron and symmetrical thickenings in both the pre- and post-synaptic membranes. Gephyrin is a post-synaptic scaffolding restricted to GABAergic synapses, and in this case to the M/T dendrites. **B.** Cross section through a M/T dendrite (pseudocolored purple) and interneuron dendritic spines (pseudocolored yellow) with two examples of reciprocal dendritic pairs labeled **i, ii.** Magnification of the corresponding synapses in panel B. In both images, the asymmetric M/T to interneuron synapse is on the left and the symmetric interneuron to M/T synapse is on the right. Arrows indicate the direction of the synapse. **C.** Another cross section through dendrites highlighting symmetric and asymmetric synapses. **D, E.** The density of asymmetric synapses is consistent throughout the EPL while the density of symmetric synapses is higher in outer than the inner EPL. **F, G.** From 64 reciprocal synapse pairs, the average length of the specialized membranes as well as the number of vesicles in the symmetric synapses are greater than that of the asymmetric synapses in both the outer and inner EPL.
Error bars indicate SEM. Abbreviations: GL, glomerular layer; EPL, external plexiform layer; MCL, mitral cell layer; GCL, granule cell layer; Glu, glutamate; asym, asymmetric synapse; sym, symmetric synapse.

Figure 3. Distribution of gephyrin-IR inhibitory synapses along M/T lateral dendrites in Tg(Thy1-YFP)GJrs tissue. The Thy1 promoter drives YFP expression in large subsets of M/T cells. **A.** YFP is shown in green, Gephyrin-IR in red, and DRAQ5 in blue, which is

used to delineate the layers of the olfactory bulb. As shown in single-plane confocal images, despite the fainter YFP staining in the outer compared to inner EPL, there was sufficient labeling to examine lateral dendrites in both outer and inner EPL. **B.** Higher resolution of the boxed region in panel A reveals it is possible to identify and measure individual dendritic segments and determine gephyrin-IR puncta that are associated with the segments in a single-plane confocal image. **C, C'.** Magnification of the boxed region in panel B with YFP in green and gephyrin in magenta. Upon delineating the boundaries of the YFP labeling, the boundaries were superimposed onto the magenta channel where the gephyrin-IR synapses were identified and counted. **D.** The gephyrin density was analyzed as a measure of the dendrite diameter; the larger diameters are closer to the somata while the smaller diameters are more distal to the somata. When the number of gephyrin-IR puncta is divided by the available length of the dendritic segment, the resulting linear density shows that segments more proximal to the somata, i.e., with a larger diameter, have the highest density of gephyrin-IR synapses. This density occurs on dendrites in both the outer and inner EPL. The slope of the line, which represents the best fit of the data by linear regression, is significantly different than 0. **E.** Considering the entire "synaptic space" of a dendritic segment and dividing the number of gephyrin-IR puncta by the surface area of the segment shows that segments more distal to the somata, and hence with a smaller diameter, have the higher density of gephyrin-IR synapses. This is true for dendrites in both the outer and inner EPL, the slope of the best-fit line is significantly different than 0.
Abbreviations: GL, glomerular layer; EPL, external plexiform layer; MCL, mitral cell layer; GCL, granule cell layer.

Figure 4. Gephyrin-IR inhibitory synapses along small populations of Lucifer-Yellow labeled M/T lateral dendrites. **A.** Injecting Lucifer Yellow into the mitral cell layer labels subsets of cells in the vicinity of the pipette, shown here in 2D confocal projections. Lucifer yellow is in green, gephyrin-IR is in red, and the nuclear stain DRAQ5 is in blue. **B.** Higher resolution of the boxed region in panel A reveals dendrites that are labeled with Lucifer Yellow. This includes granule cell dendrites but because these are characteristically spiny (arrows), we could easily avoid including them in our analysis. **C, C'.** Magnification of the boxed region in panel B with Lucifer yellow in green and gephyrin in magenta. The boundaries of the Lucifer Yellow+ dendrite were delineated and superimposed onto the magenta channel, where the gephyrin-IR puncta were identified and counted. **D.** The linear density of gephyrin-IR puncta is more or less uniform along the Lucifer Yellow dendritic segments but tends towards more gephyrin-IR puncta on dendrites with a larger diameter. The slope of the best-fit line does not differ significantly from 0. **E.** The surface area density of gephyrin-IR shows that more synapses occur on dendritic segments that have smaller diameters and, thus, are further from the cell body. The slope of the best-fit line is significantly different from 0.
Abbreviations: EPL, external plexiform layer; MCL, mitral cell layer.

Figure 5. Gephyrin-IR inhibitory synapses distributed along lateral dendrites of individually labeled mitral cells. **A.** Representative recordings of three different mitral cells in whole-cell configuration and current clamp mode showing a variety of firing

patterns. The cell at the top showed regular firing at 14 Hz; the cell in the middle showed irregular firing at 2 Hz; the cell at the bottom fired in bursts, at 16 Hz during the bursts. **B.** A single mitral cell filled with neurobiotin (green) and stained with gephyrin (red) and DRAQ5 (blue) and displayed in a 2D confocal projection. **C.** The same mitral cell in panel A reconstructed in 3D using Imaris software. **D1-4, E1-4.** Models composed from higher resolution images corresponding to boxes in panel B reveal that gephyrin-IR puncta (magenta) are non-uniformly distributed along dendrites and often occur in clusters. **F.** Analysis from six different cells shows that the linear density of gephyrin-IR puncta is mostly uniform along the dendritic segments, as the slope of the best-fit line does not differ significantly from 0. **G.** The surface area density of gephyrin-IR synapses reveals that the smaller diameter segments, and hence those more distal to the somata, have a greater synaptic density. The slope of the best-fit line is significantly different than 0.

Abbreviations: GL, glomerular layer; EPL, external plexiform layer; MCL, mitral cell layer.

REFERENCES

Au WW, Treloar HB, Greer CA. 2002. Sublaminar organization of the mouse olfactory bulb nerve layer. J Comp Neurol 446(1):68-80.

Bischofberger J, Jonas P. 1997. Action potential propagation into the presynaptic dendrites of rat mitral cells. The Journal of physiology 504 (Pt 2):359-365.

Buck L, Axel R. 1991. A novel multigene family may encode odorant receptors: a molecular basis for odor recognition. Cell 65(1):175-187.

Chen JL, Villa KL, Cha JW, So PT, Kubota Y, Nedivi E. 2012. Clustered dynamics of inhibitory synapses and dendritic spines in the adult neocortex. Neuron 74(2):361-373.

Chen WR, Midtgaard J, Shepherd GM. 1997. Forward and backward propagation of dendritic impulses and their synaptic control in mitral cells. Science 278(5337):463-467.

Cuntz H, Borst A, Segev I. 2007. Optimization principles of dendritic structure. Theoretical biology & medical modelling 4:21.

Dobrunz LE, Stevens CF. 1997. Heterogeneity of release probability, facilitation, and depletion at central synapses. Neuron 18(6):995-1008.

Donohue DE, Ascoli GA. 2008. A comparative computer simulation of dendritic morphology. PLoS computational biology 4(5):e1000089.

Druckmann S, Feng L, Lee B, Yook C, Zhao T, Magee JC, Kim J. 2014. Structured synaptic connectivity between hippocampal regions. Neuron 81(3):629-640.

Eyre MD, Antal M, Nusser Z. 2008. Distinct deep short-axon cell subtypes of the main olfactory bulb provide novel intrabulbar and extrabulbar GABAergic connections. J Neurosci 28(33):8217-8229.

Feng G, Mellor RH, Bernstein M, Keller-Peck C, Nguyen QT, Wallace M, Nerbonne JM, Lichtman JW, Sanes JR. 2000. Imaging neuronal subsets in transgenic mice expressing multiple spectral variants of GFP. Neuron 28(1):41-51.

Fogarty MJ, Hammond LA, Kanjhan R, Bellingham MC, Noakes PG. 2013. A method for the three-dimensional reconstruction of Neurobiotin-filled neurons and the location of their synaptic inputs. Frontiers in neural circuits 7:153.

Golding NL, Staff NP, Spruston N. 2002. Dendritic spikes as a mechanism for cooperative long-term potentiation. Nature 418(6895):326-331.

Greer CA. 1987. Golgi analyses of dendritic organization among denervated olfactory bulb granule cells. J Comp Neurol 257(3):442-452.

Harris KM, Weinberg RJ. 2012. Ultrastructure of synapses in the mammalian brain. Cold Spring Harbor perspectives in biology 4(5).

Hinds JW, Hinds PL. 1976a. Synapse Formation in Mouse Olfactory-Bulb .1. Quantitative Studies. J Comp Neurol 169(1):15-40.

Hinds JW, Hinds PL. 1976b. Synapse Formation in Mouse Olfactory-Bulb .2. Morphogenesis. J Comp Neurol 169(1):41-61.

Huang L, Garcia I, Jen HI, Arenkiel BR. 2013. Reciprocal connectivity between mitral cells and external plexiform layer interneurons in the mouse olfactory bulb. Frontiers in neural circuits 7:32.

Igarashi KM, Ieki N, An M, Yamaguchi Y, Nagayama S, Kobayakawa K, Kobayakawa R, Tanifuji M, Sakano H, Chen WR, Mori K. 2012. Parallel mitral and tufted cell pathways route distinct odor information to different targets in the olfactory cortex. J Neurosci 32(23):7970-7985.

Imamura F, Greer CA. 2009. Dendritic Branching of Olfactory Bulb Mitral and Tufted Cells: Regulation by TrkB. Plos One 4(8).

Imamura F, Nagao H, Naritsuka H, Murata Y, Taniguchi H, Mori K. 2006. A leucine-rich repeat membrane protein, 5T4, is expressed by a subtype of granule cells with dendritic arbors in specific strata of the mouse olfactory bulb. J Comp Neurol 495(6):754-768.

Isaacson JS, Strowbridge BW. 1998. Olfactory reciprocal synapses: dendritic signaling in the CNS. Neuron 20(4):749-761.

Jackowski A, Parnavelas JG, Lieberman AR. 1978. The reciprocal synapse in the external plexiform layer of the mammalian olfactory bulb. Brain research 159(1):17-28.

Kashiwadani H, Sasaki YF, Uchida N, Mori K. 1999. Synchronized oscillatory discharges of mitral/tufted cells with different molecular receptive ranges in the rabbit olfactory bulb. J Neurophysiol 82(4):1786-1792.

Kato HK, Gillet SN, Peters AJ, Isaacson JS, Komiyama T. 2013. Parvalbumin-expressing interneurons linearly control olfactory bulb output. Neuron 80(5):1218-1231.

Ke MT, Fujimoto S, Imai T. 2013. SeeDB: a simple and morphology-preserving optical clearing agent for neuronal circuit reconstruction. Nat Neurosci.

Kelsch W, Lin CW, Lois C. 2008. Sequential development of synapses in dendritic domains during adult neurogenesis. Proc Natl Acad Sci U S A 105(43):16803-16808.

Kosaka T, Kosaka K. 2008. Heterogeneity of parvalbumin-containing neurons in the mouse main olfactory bulb, with special reference to short-axon cells and betaIV-spectrin positive dendritic segments. Neuroscience research 60(1):56-72.

Lagier S, Carleton A, Lledo PM. 2004. Interplay between local GABAergic interneurons and relay neurons generates gamma oscillations in the rat olfactory bulb. J Neurosci 24(18):4382-4392.

Lagier S, Panzanelli P, Russo RE, Nissant A, Bathellier B, Sassoe-Pognetto M, Fritschy JM, Lledo PM. 2007. GABAergic inhibition at dendrodendritic synapses tunes gamma oscillations in the olfactory bulb. Proc Natl Acad Sci U S A 104(17):7259-7264.

Lemasson M, Saghatelyan A, Olivo-Marin JC, Lledo PM. 2005. Neonatal and adult neurogenesis provide two distinct populations of newborn neurons to the mouse olfactory bulb. J Neurosci 25(29):6816-6825.

Lepousez G, Csaba Z, Bernard V, Loudes C, Videau C, Lacombe J, Epelbaum J, Viollet C. 2010. Somatostatin interneurons delineate the inner part of the external plexiform layer in the mouse main olfactory bulb. J Comp Neurol 518(11):1976-1994.

Lisman JE, Harris KM. 1993. Quantal analysis and synaptic anatomy--integrating two views of hippocampal plasticity. Trends in neurosciences 16(4):141-147.

Lledo PM, Merkle FT, Alvarez-Buylla A. 2008. Origin and function of olfactory bulb interneuron diversity. Trends in neurosciences 31(8):392-400.

Luo M, Katz LC. 2001. Response correlation maps of neurons in the mammalian olfactory bulb. Neuron 32(6):1165-1179.

Major G, Polsky A, Denk W, Schiller J, Tank DW. 2008. Spatiotemporally graded NMDA spike/plateau potentials in basal dendrites of neocortical pyramidal neurons. J Neurophysiol 99(5):2584-2601.

Margrie TW, Sakmann B, Urban NN. 2001. Action potential propagation in mitral cell lateral dendrites is decremental and controls recurrent and lateral inhibition in the mammalian olfactory bulb. Proc Natl Acad Sci U S A 98(1):319-324.

McTavish TS, Migliore M, Shepherd GM, Hines ML. 2012. Mitral cell spike synchrony modulated by dendrodendritic synapse location. Frontiers in computational neuroscience 6:3.

Migliore M, Hines ML, McTavish TS, Shepherd GM. 2010. Functional roles of distributed synaptic clusters in the mitral-granule cell network of the olfactory bulb. Frontiers in integrative neuroscience 4:122.

Miyamichi K, Amat F, Moussavi F, Wang C, Wickersham I, Wall NR, Taniguchi H, Tasic B, Huang ZJ, He Z, Callaway EM, Horowitz MA, Luo L. 2011. Cortical representations of olfactory input by trans-synaptic tracing. Nature 472(7342):191-196.

Miyamichi K, Shlomai-Fuchs Y, Shu M, Weissbourd BC, Luo L, Mizrahi A. 2013. Dissecting local circuits: parvalbumin interneurons underlie broad feedback control of olfactory bulb output. Neuron 80(5):1232-1245.

Mombaerts P, Wang F, Dulac C, Chao SK, Nemes A, Mendelsohn M, Edmondson J, Axel R. 1996. Visualizing an olfactory sensory map. Cell 87(4):675-686.

Montague AA, Greer CA. 1999. Differential distribution of ionotropic glutamate receptor subunits in the rat olfactory bulb. J Comp Neurol 405(2):233-246.

Mori K, Kishi K, Ojima H. 1983. Distribution of dendrites of mitral, displaced mitral, tufted, and granule cells in the rabbit olfactory bulb. J Comp Neurol 219(3):339-355.

Murthy VN, Sejnowski TJ, Stevens CF. 1997. Heterogeneous release properties of visualized individual hippocampal synapses. Neuron 18(4):599-612.

Nagayama S, Enerva A, Fletcher ML, Masurkar AV, Igarashi KM, Mori K, Chen WR. 2010. Differential axonal projection of mitral and tufted cells in the mouse main olfactory system. Frontiers in neural circuits 4.

Nusser Z, Kay LM, Laurent G, Homanics GE, Mody I. 2001. Disruption of GABA(A) receptors on GABAergic interneurons leads to increased oscillatory power in the olfactory bulb network. J Neurophysiol 86(6):2823-2833.

Orona E, Rainer EC, Scott JW. 1984. Dendritic and axonal organization of mitral and tufted cells in the rat olfactory bulb. J Comp Neurol 226(3):346-356.

Pallotto M, Nissant A, Fritschy JM, Rudolph U, Sassoe-Pognetto M, Panzanelli P, Lledo PM. 2012. Early formation of GABAergic synapses governs the development of adult-born neurons in the olfactory bulb. J Neurosci 32(26):9103-9115.

Panzanelli P, Bardy C, Nissant A, Pallotto M, Sassoe-Pognetto M, Lledo PM, Fritschy JM. 2009. Early synapse formation in developing interneurons of the adult olfactory bulb. J Neurosci 29(48):15039-15052.

Panzanelli P, Perazzini AZ, Fritschy JM, Sassoe-Pognetto M. 2005. Heterogeneity of gamma-aminobutyric acid type A receptors in mitral and tufted cells of the rat main olfactory bulb. J Comp Neurol 484(1):121-131.

Parrish-Aungst S, Shipley MT, Erdelyi F, Szabo G, Puche AC. 2007. Quantitative analysis of neuronal diversity in the mouse olfactory bulb. J Comp Neurol 501(6):825-836.

Pressler RT, Strowbridge BW. 2006. Blanes cells mediate persistent feedforward inhibition onto granule cells in the olfactory bulb. Neuron 49(6):889-904.

Rall W, Shepherd GM, Reese TS, Brightman MW. 1966. Dendrodendritic synaptic pathway for inhibition in the olfactory bulb. Experimental neurology 14(1):44-56.

Rela L, Bordey A, Greer CA. 2010. Olfactory Ensheathing Cell Membrane Properties Are Shaped by Connectivity. Glia 58(6):665-678.

Richard MB, Taylor SR, Greer CA. 2010. Age-induced disruption of selective olfactory bulb synaptic circuits. P Natl Acad Sci USA 107(35):15613-15618.

Rotterman TM, Nardelli P, Cope TC, Alvarez FJ. 2014. Normal distribution of VGLUT1 synapses on spinal motoneuron dendrites and their reorganization after nerve injury. J Neurosci 34(10):3475-3492.

Sassoe-Pognetto M, Fritschy JM. 2000. Mini-review: gephyrin, a major postsynaptic protein of GABAergic synapses. The European journal of neuroscience 12(7):2205-2210.

Sassoe-Pognetto M, Frola E, Pregno G, Briatore F, Patrizi A. 2011. Understanding the molecular diversity of GABAergic synapses. Frontiers in cellular neuroscience 5:4.

Schikorski T, Stevens CF. 1997. Quantitative ultrastructural analysis of hippocampal excitatory synapses. J Neurosci 17(15):5858-5867.

Schikorski T, Stevens CF. 1999. Quantitative fine-structural analysis of olfactory cortical synapses. Proc Natl Acad Sci U S A 96(7):4107-4112.

Schmidt TM, Kofuji P. 2011. Structure and function of bistratified intrinsically photosensitive retinal ganglion cells in the mouse. J Comp Neurol 519(8):1492-1504.

Schneider Gasser EM, Straub CJ, Panzanelli P, Weinmann O, Sassoe-Pognetto M, Fritschy JM. 2006. Immunofluorescence in brain sections: simultaneous detection of presynaptic and postsynaptic proteins in identified neurons. Nature protocols 1(4):1887-1897.

Schoppa NE, Urban NN. 2003. Dendritic processing within olfactory bulb circuits. Trends in neurosciences 26(9):501-506.

Shepherd GM, Chen WR, Greer CA. 2004. Olfactory bulb. In: Shepherd GM, ed. The Synaptic Organization of the Brain. 5th ed. New York: Oxford University Press.

Sosulski DL, Bloom ML, Cutforth T, Axel R, Datta SR. 2011. Distinct representations of olfactory information in different cortical centres. Nature 472(7342):213-216.

Specht CG, Izeddin I, Rodriguez PC, El Beheiry M, Rostaing P, Darzacq X, Dahan M, Triller A. 2013. Quantitative nanoscopy of inhibitory synapses: counting gephyrin molecules and receptor binding sites. Neuron 79(2):308-321.

Steward O, Wallace CS, Lyford GL, Worley PF. 1998. Synaptic activation causes the mRNA for the IEG Arc to localize selectively near activated postsynaptic sites on dendrites. Neuron 21(4):741-751.

Tan J, Savigner A, Ma M, Luo M. 2010. Odor information processing by the olfactory bulb analyzed in gene-targeted mice. Neuron 65(6):912-926.

Toida K, Kosaka K, Heizmann CW, Kosaka T. 1994. Synaptic contacts between mitral/tufted cells and GABAergic neurons containing calcium-binding protein parvalbumin in the rat olfactory bulb, with special reference to reciprocal synapses between them. Brain research 650(2):347-352.

Treloar HB, Feinstein P, Mombaerts P, Greer CA. 2002. Specificity of glomerular targeting by olfactory sensory axons. J Neurosci 22(7):2469-2477.

Whitman MC, Greer CA. 2007. Synaptic integration of adult-generated olfactory bulb granule cells: Basal axodendritic centrifugal input precedes apical dendrodendritic local circuits. J Neurosci 27(37):9951-9961.

Whitman MC, Greer CA. 2009. Adult neurogenesis and the olfactory system. Prog Neurobiol 89(2):162-175.

Woolf TB, Shepherd GM, Greer CA. 1991. Serial reconstructions of granule cell spines in the mammalian olfactory bulb. Synapse 7(3):181-192.

Xiong W, Chen WR. 2002. Dynamic gating of spike propagation in the mitral cell lateral dendrites. Neuron 34(1):115-126.

Yokoi M, Mori K, Nakanishi S. 1995. Refinement of odor molecule tuning by dendrodendritic synaptic inhibition in the olfactory bulb. Proc Natl Acad Sci U S A 92(8):3371-3375.

Zhang J, Zhang AJ, Wu SM. 2006. Immunocytochemical analysis of GABA-positive and calretinin-positive horizontal cells in the tiger salamander retina. J Comp Neurol 499(3):432-441.

Zhang X, Firestein S. 2002. The olfactory receptor gene superfamily of the mouse. Nat Neurosci 5(2):124-133.

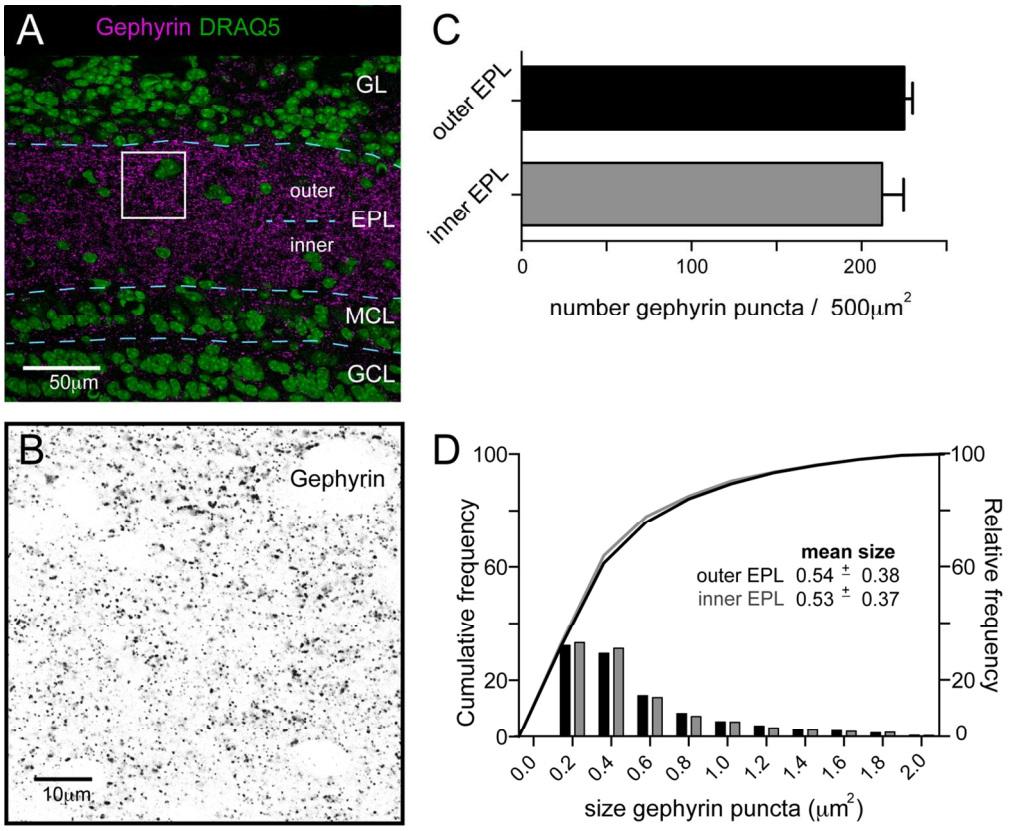

Inhibitory synaptic distribution throughout the external plexiform layer (EPL) as seen by staining for gephyrin, a post-synaptic marker of GABAergic synapses. A. Gephyrin-IR (immunoreactivity, in magenta) appears punctate and uniform throughout the EPL. Layers within the olfactory bulb are visualized and delineated with the DRAQ5 nuclear stain (green). B. Staining from boxed region in panel A; Gephyrin was imaged at higher resolution and the gray-scale inverted images were used to analyze puncta. C. The density of gephyrin-IR puncta is uniform across the outer EPL (black bar) and inner EPL (grey bar). D. The mean size of gephyrin-IR puncta is 0.5μm; cumulative and relative frequencies are also shown. Error bars indicate SEM. Abbreviations: GL, glomerular layer; EPL, external plexiform layer; MCL, mitral cell layer; GCL, granule cell layer.

129x107mm (300 x 300 DPI)

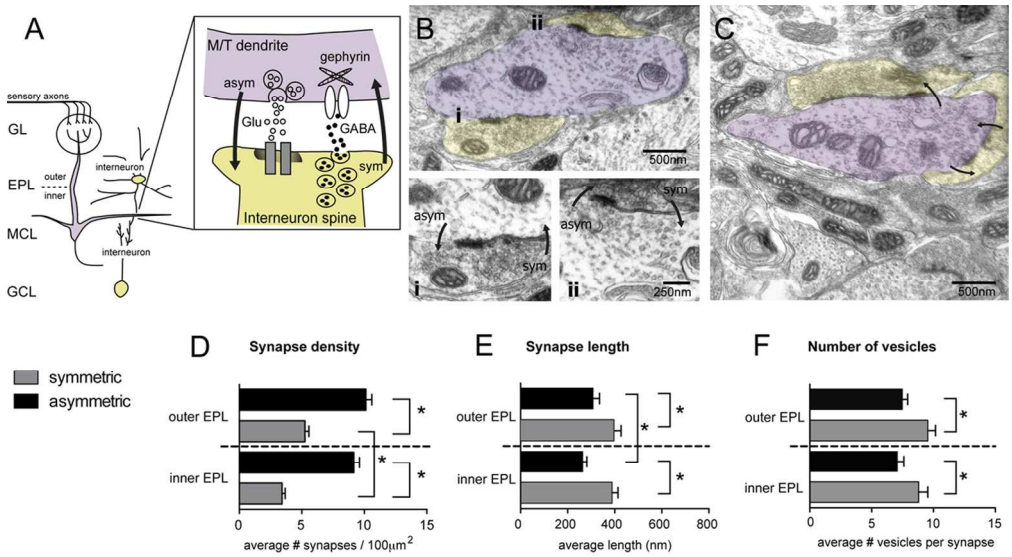

Dendrodendritic synapses in the EPL. A. A simplified circuit of the olfactory bulb. The mitral/tufted cells (M/T; purple) extend their primary dendrite into glomeruli where they receive input from the axon terminals of olfactory sensory neurons. Along the M/T secondary dendrites, which extend laterally through the EPL, dendrodendritic synapses are formed with interneurons (yellow). These synapses occur primarily with granule cells, located deep in the granule cell layer, and possibly with various interneuron populations within the EPL. Box inset: The dendrodendritic microcircuit begins at the asymmetric synapses with the M/T release of glutamate onto interneuron dendritic spines. This synapse is defined by ¬vesicles closely apposed to the M/T presynaptic membrane and an asymmetrically thick post-synaptic specialization on the interneuron membrane. The reciprocal symmetric synapse entails vesicle clusters throughout the spine of the interneuron and symmetrical thickenings in both the pre- and post-synaptic membranes. Gephyrin is a post-synaptic scaffolding restricted to GABAergic synapses, and in this case to the M/T dendrites. B. Cross section through a M/T dendrite (pseudocolored purple) and interneuron dendritic spines (pseudocolored yellow) with two examples of reciprocal dendritic pairs labeled i, ii. Magnification of the corresponding synapses in panel B. In both images, the asymmetric M/T to interneuron synapse is on the left and the symmetric interneuron to M/T synapse is on the right. Arrows indicate the direction of the synapse. C. Another cross section through dendrites highlighting symmetric and asymmetric synapses. D, E. The density of asymmetric synapses is consistent throughout the EPL while the density of symmetric synapses is higher in outer than the inner EPL. F, G. From 64 reciprocal synapse pairs, the average length of the specialized membranes as well as the number of vesicles in the symmetric synapses are greater than that of the asymmetric synapses in both the outer and inner EPL.
Error bars indicate SEM. Abbreviations: GL, glomerular layer; EPL, external plexiform layer; MCL, mitral cell layer; GCL, granule cell layer; Glu, glutamate; asym, asymmetric synapse; sym, symmetric synapse.

129x71mm (300 x 300 DPI)

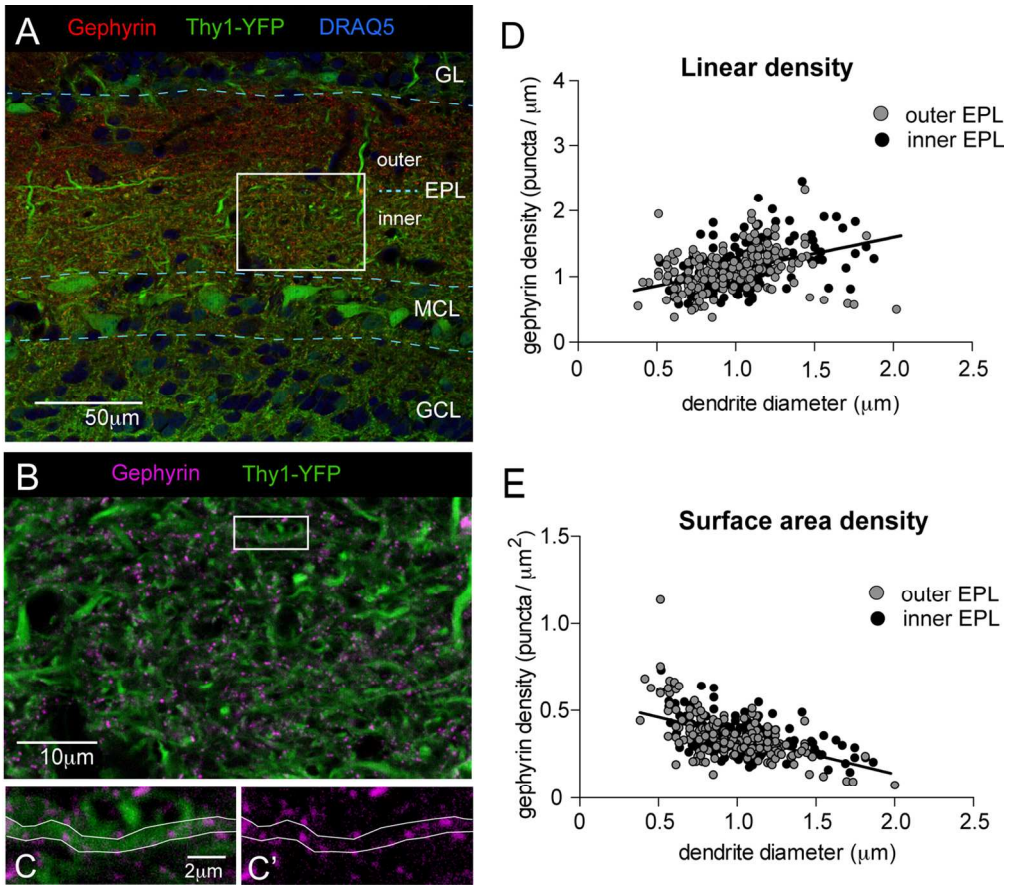

Distribution of gephyrin-IR inhibitory synapses along M/T lateral dendrites in Tg(Thy1-YFP)GJrs tissue. The Thy1 promoter drives YFP expression in large subsets of M/T cells. A. YFP is shown in green, Gephyrin-IR in red, and DRAQ5 in blue, which is used to delineate the layers of the olfactory bulb. As shown in single-plane confocal images, despite the fainter YFP staining in the outer compared to inner EPL, there was sufficient labeling to examine lateral dendrites in both outer and inner EPL. B. Higher resolution of the boxed region in panel A reveals it is possible to identify and measure individual dendritic segments and determine gephyrin-IR puncta that are associated with the segments in a single-plane confocal image. C, C'. Magnification of the boxed region in panel B with YFP in green and gephyrin in magenta. Upon delineating the boundaries of the YFP labeling, the boundaries were superimposed onto the magenta channel where the gephyrin-IR synapses were identified and counted. D. The gephyrin density was analyzed as a measure of the dendrite diameter; the larger diameters are closer to the somata while the smaller diameters are more distal to the somata. When the number of gephyrin-IR puncta is divided by the available length of the dendritic segment, the resulting linear density shows that segments more proximal to the somata, i.e., with a larger diameter, have the highest density of gephyrin-IR synapses. This density occurs on dendrites in both the outer and inner EPL. The slope of the line, which represents the best fit of the data by linear regression, is significantly different than 0. E. Considering the entire "synaptic space" of a dendritic segment and dividing the number of gephyrin-IR puncta by the surface area of the segment shows that segments more distal to the somata, and hence with a smaller diameter, have the higher density of gephyrin-IR synapses. This is true for dendrites in both the outer and inner EPL, the slope of the best-fit line is significantly different than 0.
Abbreviations: GL, glomerular layer; EPL, external plexiform layer; MCL, mitral cell layer; GCL, granule cell layer.

129x114mm (300 x 300 DPI)

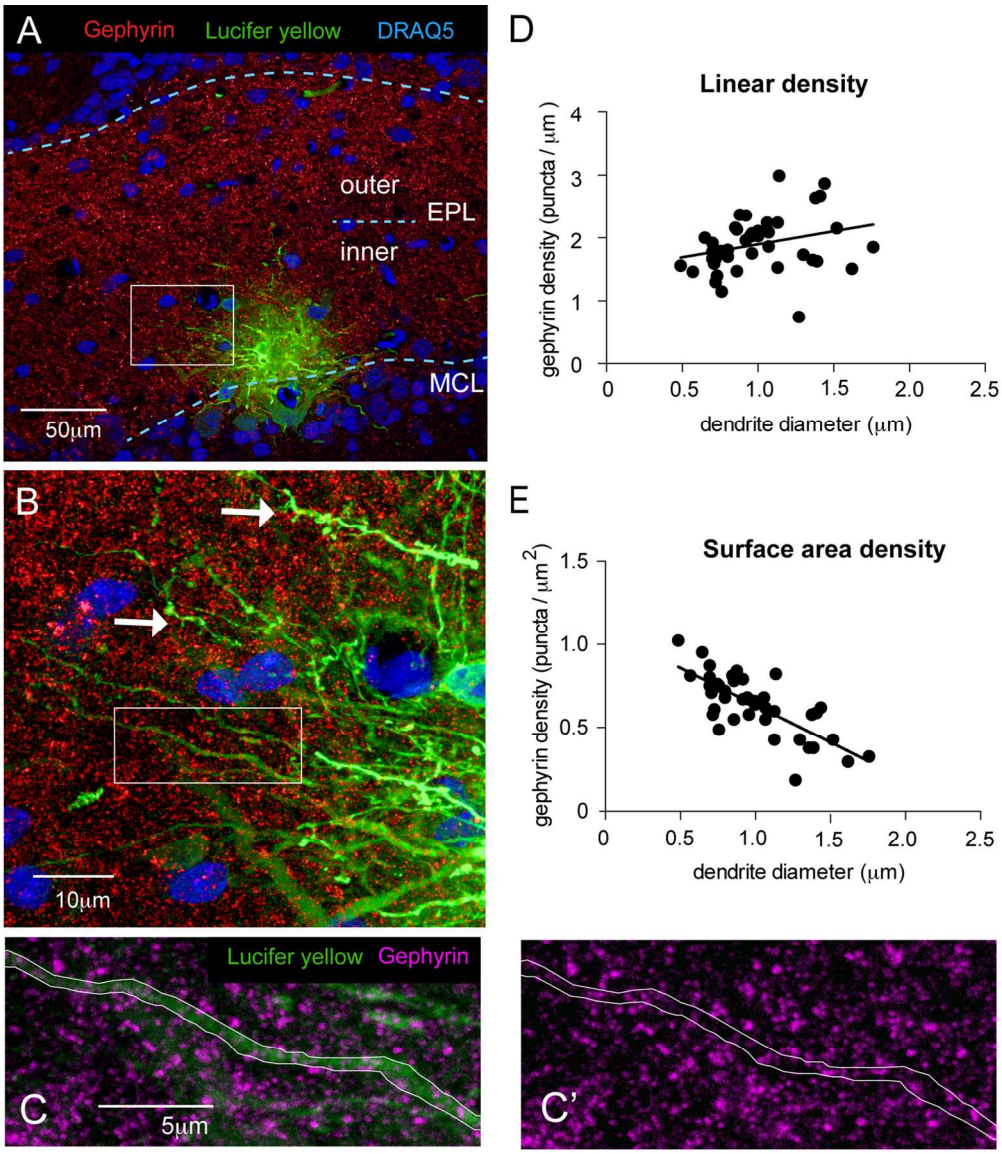

Gephyrin-IR inhibitory synapses along small populations of Lucifer-Yellow labeled M/T lateral dendrites. A. Injecting Lucifer Yellow into the mitral cell layer labels subsets of cells in the vicinity of the pipette, shown here in 2D confocal projections. Lucifer yellow is in green, gephyrin-IR is in red, and the nuclear stain DRAQ5 is in blue. B. Higher resolution of the boxed region in panel A reveals dendrites that are labeled with Lucifer Yellow. This includes granule cell dendrites but because these are characteristically spiny (arrows), we could easily avoid including them in our analysis. C, C'. Magnification of the boxed region in panel B with Lucifer yellow in green and gephyrin in magenta. The boundaries of the Lucifer Yellow+ dendrite were delineated and superimposed onto the magenta channel, where the gephyrin-IR puncta were identified and counted. D. The linear density of gephyrin-IR puncta is more or less uniform along the Lucifer Yellow dendritic segments but tends towards more gephyrin-IR puncta on dendrites with a larger diameter. The slope of the best-fit line does not differ significantly from 0. E. The surface area density of gephyrin-IR shows that more synapses occur on dendritic segments that have smaller diameters and, thus, are further from the cell body. The slope of the best-fit line is significantly different from 0.
Abbreviations: EPL, external plexiform layer; MCL, mitral cell layer.

129x149mm (300 x 300 DPI)

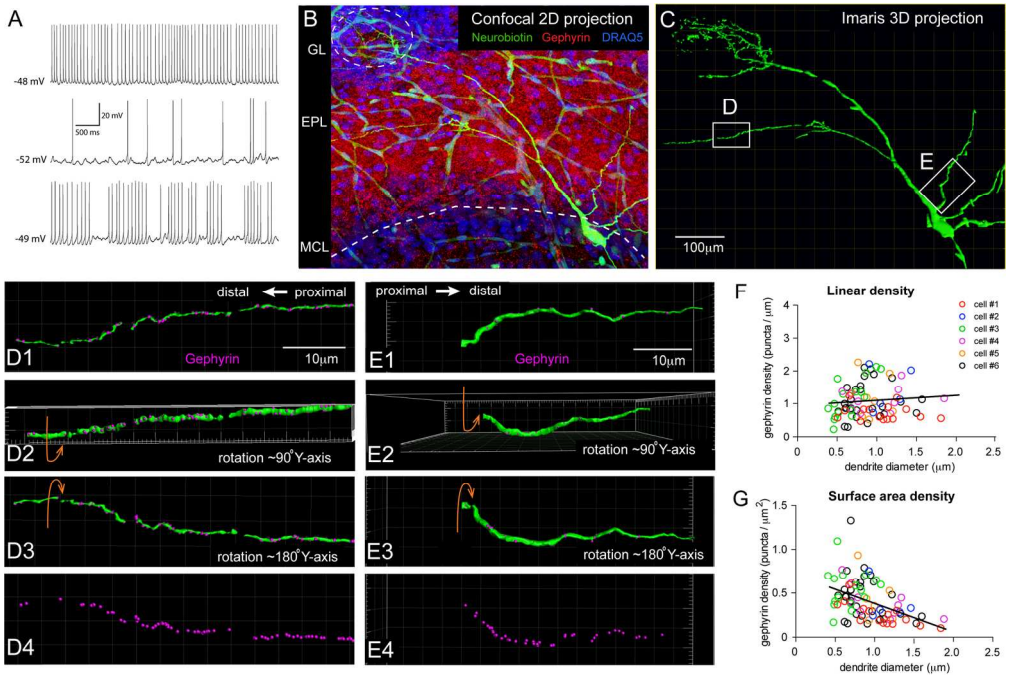

Gephyrin-IR inhibitory synapses distributed along lateral dendrites of individually labeled mitral cells. A. Representative recordings of three different mitral cells in whole-cell configuration and current clamp mode showing a variety of firing patterns. The cell at the top showed regular firing at 14 Hz; the cell in the middle showed irregular firing at 2 Hz; the cell at the bottom fired in bursts, at 16 Hz during the bursts. B. A single mitral cell filled with neurobiotin (green) and stained with gephyrin (red) and DRAQ5 (blue) and displayed in a 2D confocal projection. C. The same mitral cell in panel A reconstructed in 3D using Imaris software. D1-4, E1-4. Models composed from higher resolution images corresponding to boxes in panel B reveal that gephyrin-IR puncta (magenta) are non-uniformly distributed along dendrites and often occur in clusters. F. Analysis from six different cells shows that the linear density of gephyrin-IR puncta is mostly uniform along the dendritic segments, as the slope of the best-fit line does not differ significantly from 0. G. The surface area density of gephyrin-IR synapses reveals that the smaller diameter segments, and hence those more distal to the somata, have a greater synaptic density. The slope of the best-fit line is significantly different than 0.
Abbreviations: GL, glomerular layer; EPL, external plexiform layer; MCL, mitral cell layer.

171x115mm (300 x 300 DPI)

Table 1. Antibodies and other stains

Primary Antiserum	**Immunogen**	**Company** (catalog number) RRID	**Working dilution**
Gephyrin, mouse monoclonal IgG_1 subtype	Purified rat gephyrin N-terminus	Synaptic Systems; Goettingen, Germany (147 011) RRID:AB_887717	1:750
GFP, chicken polyclonal	Recombinant GFP	AbCam; Cambridge, MA (ab13970) RRID:AB_300798	1:1,000
Lucifer Yellow, rabbit polyclonal	Lucifer Yellow	Invitrogen; Carlsbad, CA (A5750) RRID:AB_1501344	1:1,000
Secondary Antiserum	**Conjugated to**		
donkey anti-mouse IgG_1	Alexa555	Invitrogen Carlsbad, CA (#A21127) RRID:AB_141596	1:1,000
goat anti-chicken	Alexa488	Invitrogen (#A21042) RRID:AB_141357	1:1,000
goat anti-rabbit	Alexa488	Invitrogen (A11034) RRID:AB_10562715	1:1,000
Other Stains			
Streptavidin conjugated to Alexa-488		Invitrogen (#S11223) RRID:AB_2336881	1:1,000
DRAQ5, far red nuclear stain		Biostatus Ltd; Leicestershire, UK (DR50050) RRID:AB_2314341	1:1,000

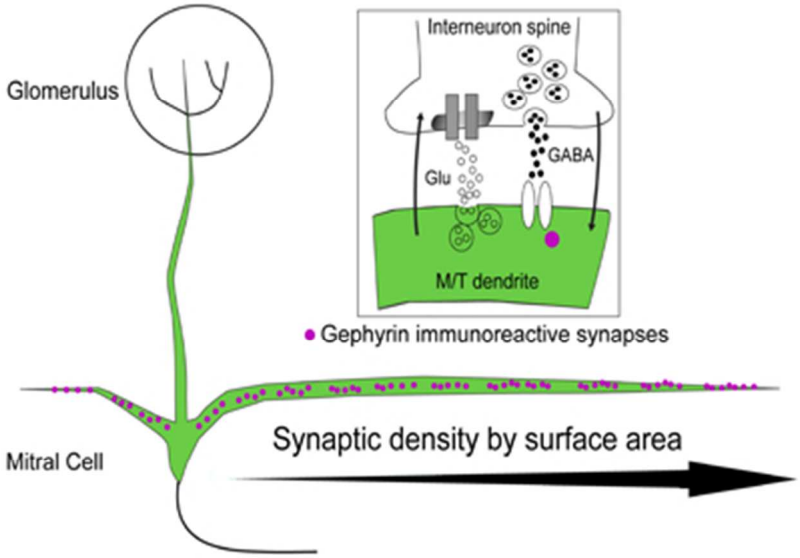

Gephyrin immunoreactive appositions, a proxy for dendrodendritic synapses along mitral cell secondary dendrites, appear in clusters with intervening membrane devoid of synapses. The absolute, or linear, synaptic density is constant along the length of dendrites. Yet when expressed as a function of surface area, the synaptic density increases distally as dendrites taper toward the terminal end.
141x105mm (72 x 72 DPI)

Gephyrin immunoreactive appositions, a proxy for dendrodendritic synapses along mitral cell secondary dendrites, appear in clusters with intervening membrane devoid of synapses. The absolute, or linear, synaptic density is constant along the length of dendrites. Yet when expressed as a function of surface area, the synaptic density increases distally as dendrites taper toward the terminal end.

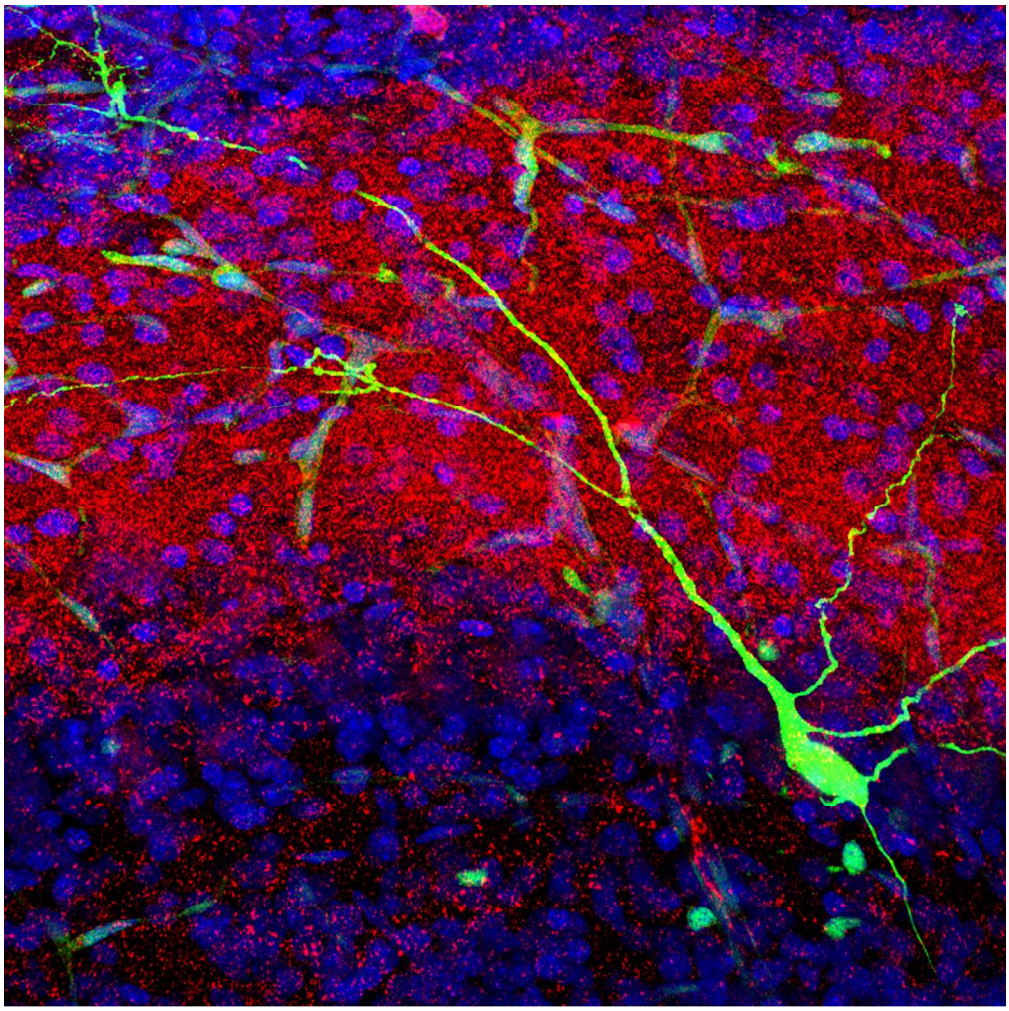

An individual mitral cell in the olfactory bulb filled with neurobiotin (green). The slice was subsequently stained with gephyrin (red, a post-synaptic marker that serves as a proxy to identify dendrodendritic synapses) and DRAQ5 (blue, nucleic counterstain to delineate the layers of the olfactory bulb). Gephyrin immunoreactivity is uniformly distributed throughout the external plexiform layer, where the secondary dendrites of mitral cells are located. However, analysis of gephyrin distribution along individual mitral cell secondary dendrites revealed that the density of gephyrin increases distally as dendrites taper away from the cell body.
199x199mm (300 x 300 DPI)

Cover image caption

An individual mitral cell in the olfactory bulb filled with neurobiotin (green). The slice was subsequently stained with gephyrin (red, a post-synaptic marker that serves as a proxy to identify dendrodendritic synapses) and DRAQ5 (blue, nucleic counterstain to delineate the layers of the olfactory bulb). Gephyrin immunoreactivity is uniformly distributed throughout the external plexiform layer, where the secondary dendrites of mitral cells are located. However, analysis of gephyrin distribution along individual mitral cell secondary dendrites revealed that the density of gephyrin increases distally as dendrites taper away from the cell body.